Policy Research Journal
ISSN (E): 3006-7030 ISSN (P) : 3006-7022 Volume 3, Issue 11, 2025

FABRICATION OF HYPERTHERMIA EFFICIENCY MEASUREMENT SYSTEM BASED ON AN ALTERNATING MAGNETIC FIELD

Fahad Rasheed[*1], Ahmad Luqman[2], Aftab Ahmed[3], Saba Batool[4], Ghulam Safia[5]

[*1,5]*University of Agriculture Faisalabad Department of Physics M.Phil. Physics*
[2,3]*Hubei Key Laboratory of Plasma Chemistry and Advanced Materials, School of Materials Science and Engineering, Wuhan Institute of Technology, Wuhan, Hubei, China, 430205*
[4]*Department name of Physics, solid state physics Lab Punjab university Lahore*

[*1]fahadrasheedqadri@hotmail.com, [2]linf9510@gmail.com, davidxaan175@gmail.com, [4]saba.batool1174@gmail.com, [5] ghulamlsafia716@gmail.com

DOI: https://doi.org/10.5281/zenodo.17761359

Keywords
Magnetic Hyperthermia, Alternating Magnetic Field (AMF), Specific Absorption Rate (SAR), Nanoparticles, Waveform Control, Thermal Efficiency, System Design

Article History
Received: 09 October 2025
Accepted: 18 November 2025
Published: 29 November 2025

Corresponding Author: *
Fahad Rasheed

Abstract
The development of magnetic hyperthermia machines is also necessary in the exact description of the heating performance of the magnetic nanoparticles (MNPs) in the presence of alternating magnetic fields (AMFs). The paper presents a report of the design, fabrication, and validation of a low-set up cost, versatile AMF system designed to produce sinusoidal and non-sinuoidal waveforms (triangular, trapezoidal, trapezoidal- triangular and sawtooth). The fabricated apparatus incorporates a full-bridge inverter AMF generator, maximized copper induction coil, fiber optic temperature detection apparatus as well as a thermally insulated three-layer calorimeter to be precisely measured. Superparamagnetic iron oxide nanoparticles (SPIONs) produced through Massart co-precipitation technique was assessed on heating performance under controlled conditions of AMF. Findings indicated how the non-sinusoidal waveforms greatly increased the heating efficiency such that the SAR was up to 45 percent higher than when using the conventional sinusoidal waveform with 200 kHz and 2.14 mT. This system showed a linear behaviour to the change in magnetic field intensity, frequency and concentration of nanoparticles, which demonstrates high stability and reproducibility of the system. Also, the analysis of waveforms indicated that it was logarithmically correlated that field rise rate was related to thermal power dissipation. Proved to be a cost-effective as well as flexible substitute to commercial systems, this open-source and modular format can allow promote deeper studies into magnetic heating systems and AMF optimization aimed at biomedical and material science purposes.

INTRODUCTION

Improvement of the medical and materials research is more and more reliant on more accurate and dependable instrumentation that has the ability to recreate complex physical situations. A particularly popular of these is magnetic hyperthermia experiment which uses precise systems to produce, direct, and measure alternating magnetic fields (AMFs) in order to determine the efficiency of magnetic nanoparticles (MNPs) in heating [1,2]. The performance of hyperthermia can generally be related to the specific absorption rate (SAR) that is the amount of thermal energy emitted by the nanoparticles at a given mass when subject to an AMF. Measurement of SAR is thus critical in determining performance of materials, testing of theoretical models and enhancement of syntheses of magnetic nanoparticles [3].

Most current hyperthermia systems, however, typically use limited-frequency AC generators, traditional sinusoidal magnetic fields and error-prone low-tech temperature measuring tools [4]. Such systems are largely unbendable in generating waveforms, in field intensity regulation and long duration thermal stability thus, inefficiently estimating efficiency. Additionally, the majority of commercial devices are costly, complicated, thus, hampering customization that should be easily done, thus making them less applicable in academic and experimental laboratories [5]. There is, therefore, an increasing need to come up with a designing and production of an effective cost and flexible measurement of the therm efficiency that is able to give a high precision and reproducibility in the laboratory scale studies [6].

Alternating magnetic field (AMF) is an important aspect of the thermal behavior of the materials which are magnetic materials. The characteristics influencing heat are the amplitude of the field, frequency, and characteristics of the waveform [7]. Although sinusoidal waveforms are standard, according to the recent findings, signals that are not sinusoidal like square or triangular waves also can be used to optimize heating, since they may contain high-frequency harmonics [8,9]. But still, no experimental systems have been developed to able to generate such variable AMF profiles and be able to remain able to monitor the induced temperature increase with adequate precision [10]. This inspires the design of a system that is capable of producing different field patterns to study their impact on performance of heating magnet materials [11].

An electrical, electronic, and thermal system should also be well incorporated to create such a system. The AMF generator, copper induction coil, cooling parts that also provide stability to the system and temperature sensing modules that also perform real-time monitoring are its main components [12]. The AMF generator should be designed to operate in the range of several hundreds of kilohertz to few kilohertz with amplitude that is variable such that it operates with different magnetic nanoparticles [13]. Power amplifier, signal control interface and shielding are also expected to be in the system, so as to diminish the impact of the electromagnetic interference [14].

The design of the induction coil which would control the field distribution and the field strength at the sample position is one of the most significant aspects of the process of fabrication. The coil geometry in relation to the number of turns and the radius of wire and radius of space has a direct effect on the uniformity of the magnetic field and homogeneous heating [15]. Analytical modeling and simulation can be used to guide the optimization of these parameters with the aid of the tools of COMSOL Multiphysics or ANSYS Maxwell before the experimental assembly is invested in [16]. It is also essential to take into consideration thermal management in a way that does not allow hot coils to function and allows stable functioning even in case of long test time [17].

A non-contact, infrared sensors, fiber optic probes and digital thermocouples can be included to the system in order to get temperature [18]. These sensors have an interface with microcontroller or data acquisition system (DAQ) to PC interface which in turn measures and logs the changes in real time in temperature or logs them to PC system [19]. It is not only more accurate, but also this automation can allow monitoring at any time and conducting comparative research on different samples and AMF conditions [20].

After being fabricated, the system has to be calibrated and validated with reference to standard magnetic materials which have known sizable SAR values [21]. This guarantees that the generated AMF is reflective of the field strength as calculated on theory as well as temperature measurements are known to be both physically consistent. Frequency behaviour of the system to different frequencies of the variable under test as well as field intensities must also be defined so as to establish that the system is linear and reliable in its operation [22]. The characteristics that are essential are the efficiency and stability of the AMF source since distortion or instability may cause large deviations to thermal measurements [23].

Besides testing it experimentally, the fabrication efficiency and cost-effectiveness of the system should also be measured. The design with simple components, which are easily accessible like electronic parts, modular circuit design, and open-source control software minimizes the production cost of using commercially available hyperthermia systems by a large margin [24]. These are accomplished by the capability of modifying or upgrading subsystems, i. e. waveform control modules or temperature sensors, to improve the research value of the system in the long term [25]. Moreover, the modular design allows solving the extension to the biomedical or materials testing in the future [26].

The major aim of the current study is thus to design, manufacture and test an alternating magnetic field with variable waveform control and a scale size laboratory complete system to measure the efficiency of heat generation. The developed artificial system is out to generate AMF fields of adjustable frequency and intensity, quantify the related thermal reaction of organic materials, and develop a reasonable relationship between the magnetic parameters and warming proficiency [27]. In the end, this system offers an easy and cost effective means of examining thermal characteristics in nanoparticles, magnetic composites and ferrofluids and thus it will help in generating better materials engineering techniques and applied magnetic studies [28-30].

2. Materials and Methods

2.1. Materials

The measurement system of hyperthermia efficiency that was invented in this research is made up of an alternating magnetic field (AMF) generator, an optimized induction coil, a fiber optic system of temperature measurement, and a multilayer calorimetric sample holder. The system is set up in such a way that the efficiency of heating magnetic nanoparticles (MNPs) in different waveform excitations can be assessed. The whole setup layers in real-time temperature, controlled waveforms with precision and thermal isolation in properly characterizing magnetic hyperthermia performance.

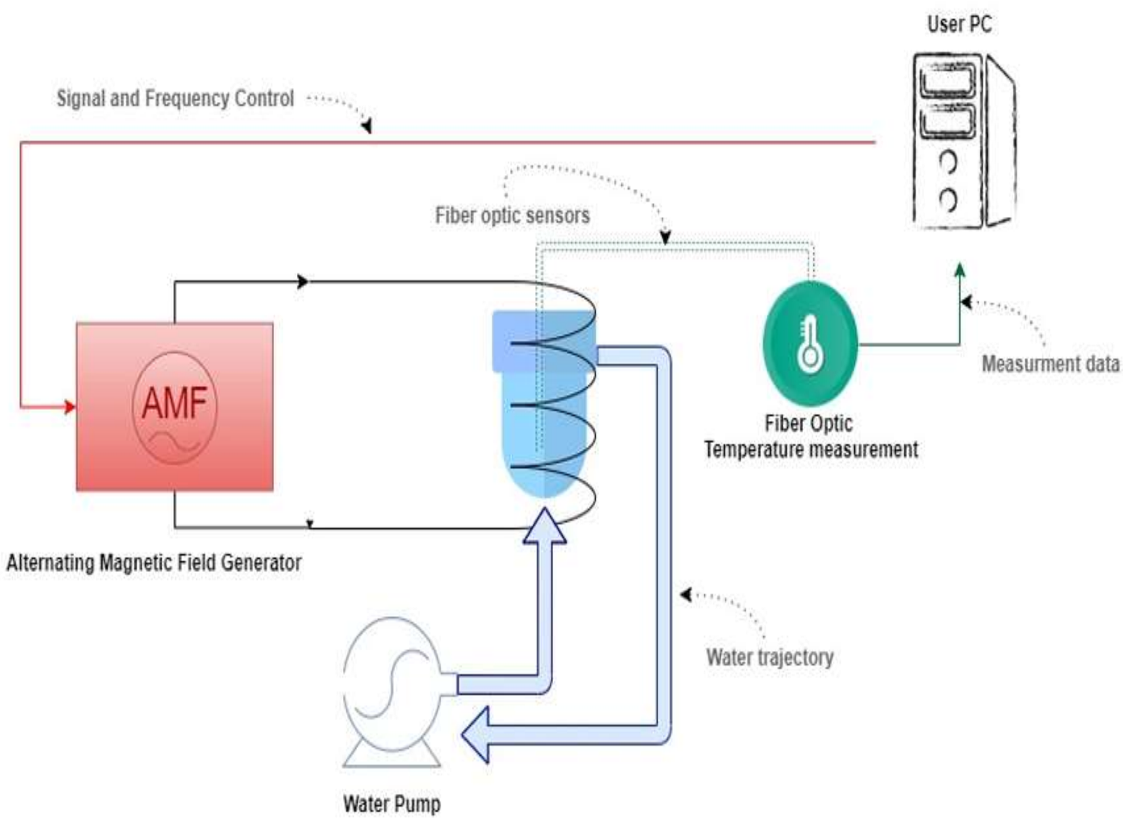

Figure 1. Hyperthermia system workflow.

2.1.1. Strong magnetic field (AMF) Generator.

In this study, the AMF generator that was used was a full-bridge inverter-based generator created in the laboratory. It can generate four non-standard waveforms, such as triangular (TR), trapezoidal-triangular (TT), trapezoidal (TP) and trapezoidal-square (TS) waveforms as well as a normal sinusoidal (SN) waveform in order to provide a point of comparison. The highest current that the generator can give is 100 Apk-pk and the range of frequencies that can be applied can be in between 1 MHz and 100 kHz with the step size being 100 kHz. The irregular waveforms were produced in the study of the effects of variations in slope of the magnetic fields to the heating efficiency of nanoparticles.

Design Coil In design Optimization was performed on the design of coils previously optimized, resulting in an AMF method that is up to 3.2 mT with an input current of 30 Apk-pk. Yet because of thermal considerations, which were met through the current limitation, the current was used in a stabilized manner. The coil and AMF generator specifications have been tested by waveform technology using oscilloscopes to see that the generator was capable of creating steady signal at all frequencies processed.

2.1.2. Fiber Optic Temperature Metering Schematic.

An AMF environment results in the need of non-metallic and interference-free sensors to determine temperature. Therefore, Luxtron 3300 fiber optic sensors were used in the determination of thermal values with greater precision. The temperature variations present in a set position, in each sensor channel are all recorded simultaneously in multiple positions of the sensor channels; in the nanoparticle-sample, in the encircling fluid and in the surrounding environment.

The sample was placed in a sample tube and a Pasteur pipette was inserted to keep the fiber optic sensor in the geometrical centre of the sample so that the temperature would be measured consistently regardless of the gradient in the convection. Also with this design immunity to cable bending and reproducibility with tests is possible.

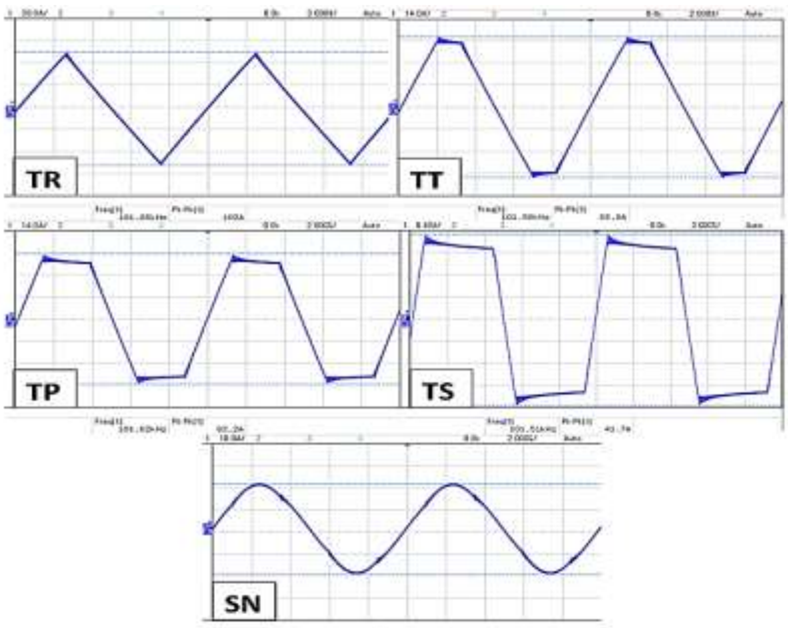

Figure 2. AMF generator waveforms.

2.1.3. Calorimeter Design

An instrument of tri-layers calorimeter was designed to remove the presence of outside heat in the coil, and create the required controlled environment. It consisted of: an outer water circulation system kept at 37 degC by a constant supply of water pump. A vacuum insulation to reduce heat transfer and a suspension chamber of nanoparticles on the inside are also present. This system prevented the test sample to be subjected to effects of third parties with regard to temperature variation. The confirmation of validation with the deionized water at constant temperature of the coil showed that the temperature of the coil increased to 150 degC, and the temperature of the sample was constant at 37 degC, converting to chemical signal that also indicates that there was good isolation performance.

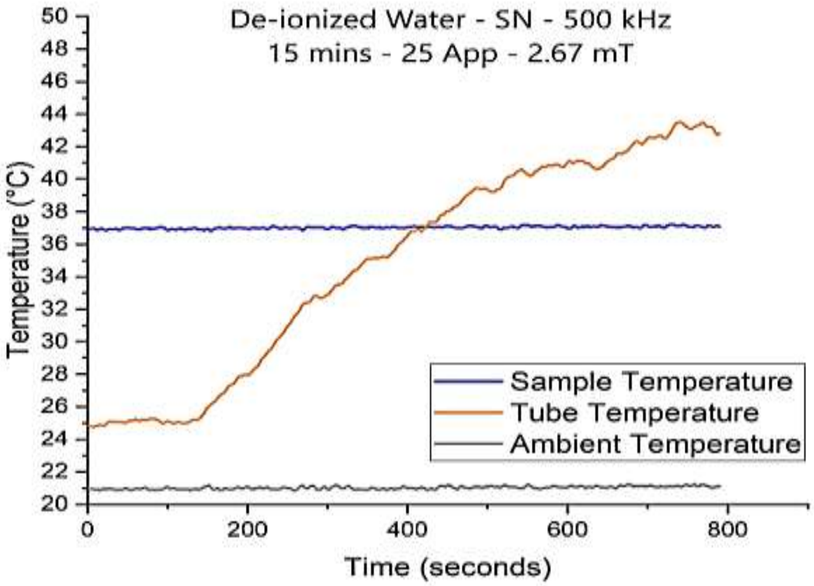

Figure 3. Sample temperature isolation test using de-ionized water

2.1.4. Nanoparticle Synthesis

Ten nanometers Massart co-precipitation method of synthesizing SPIONs with an average diameter of 10 nm was used. An aliquot of 0.09 of ferric chloride (FeCl36H2O, 0.09 mol) and 0.054 mol of ferrous chloride (FeCl24H2O) was added to the stirring of the 3.4% ammonium hydroxide to a standing with a very violent stirring. The precipitate was ground in trio of pipettings of distilled water, later shaken decantedly (still in 2M-NO3) and precipitate in regard was subjected to 2M nitric acid two musings after which 1M Fe(NO3)3 was added to ascertain the purity of the particles.

Sonication in water was harshly used to redispersed the final product resulting in colloidal suspension of 75 mg Fe/mL. The hydrodynamic diameter of the particles was 47.6nm, PDI=0.23, and the zeta potential was +21 mV at pH 3. The sphericity and steep size assessment were verified by transmission electron microscopy (TEM).

2.2. Experimental Methods

2.2.1. Sample Preparation

For each test, **500 µL** of the SPION suspension was transferred into a **177.8 mm × 5 mm** glass tube. Samples were ultrasonicated for **90 s at 37 °C** to disperse agglomerates before placement into the calorimeter. The sample position was carefully aligned with the coil center to ensure uniform magnetic exposure. Water circulation maintained the sample at 37 °C prior to the start of measurements, simulating physiological conditions.

2.2.2. Exposure to Alternating Magnetic Field

Once temperature stabilization was confirmed, the AMF generator was activated with the selected waveform and frequency. Simultaneously, the fiber optic sensors recorded temperature data at **1 s intervals** for a total duration of **900 s**. After field exposure, temperature recording continued during the natural cooling phase to generate the full heating-cooling cycle curve.

2.2.3. Data Acquisition and Processing

All recorded temperature data were exported to **Microsoft Excel** for organization and subsequently analyzed using **OriginPro software** for curve fitting.
The temperature evolution was modeled using the exponential fitting function:
[T = T_0 + \Delta T (1 - e^{-t / \tau})]
where **T** is temperature at time *t*, $\mathbf{T_0}$ is the initial temperature, **ΔT** is the steady-state temperature change, and **τ** is the characteristic time constant. A **cast-out approach** was applied to determine a representative τ value for all curves, improving the reliability of fitting results.

2.2.4. Waveform Slope Analysis

The **waveform slope** (S) was determined using the relation:
[S = H_{ac} \times f \times S_f]
where $\mathbf{H_{ac}}$ is the magnetic field amplitude, **f** is frequency, and **S_f** is the waveform-specific slope factor. The **S_f** values were experimentally determined using an oscilloscope for each waveform type (SN, TR, TT, TP, TS). These slope values quantified the magnetic rise and fall times influencing heating dynamics.

2.2.5. Normalized Thermal Power Increment

The **normalized thermal power increment** ($P_{i,j}$) between two waveforms was calculated as:
[P_{i,j} = \frac{\Delta T_i}{\Delta T_j} - 1]
This ratio represents the relative heating efficiency of two different waveforms under similar experimental conditions, providing insights into the influence of magnetic field slope on nanoparticle heating behavior.

3. Results

These experiments were done to test the ability of the fabricated system of hyperthermia efficiency measurement to work under different strength of magnetic field, frequency and nanoparticle (NP) concentration. This was aimed at analyzing the heating response, thermal power and normalized dissipation with the use of conventional(sinuoidal) and non-conventional (triangular, trapezoidal and sawtooth) AMF waves. Each test took a 900 s period to operate the experimental setup, and the ultimate increase in temperature was termed as power dissipation and specific absorption rate (SAR) was computed based on a formula (Equation 6).**3.1.**

Effect of Intensity of Magnetic Field.

The dependence of AMF strength versus temperature increase was studied by changing magnetic field to 0.5 Mt up to 3.2 Mt with a constant frequency of 100 KHz in nanoparticle suspensions of 75 mgFe/Ml. The findings included that there is an inverse relationship between the strength of the magnetic field and a decrease in temperature. Out of all the tested waveforms the triangular (TS) and a trapezoidal (TP) signals had better heating characteristics compared to the 699inusoidal (SN) waveform. This verifies that the slope of the waveforms has a vital effect on heating efficiency because greater hexahedral induce a higher level of the eddy currents and hysteresis throughput in the nanoparticles as in table 3.1.

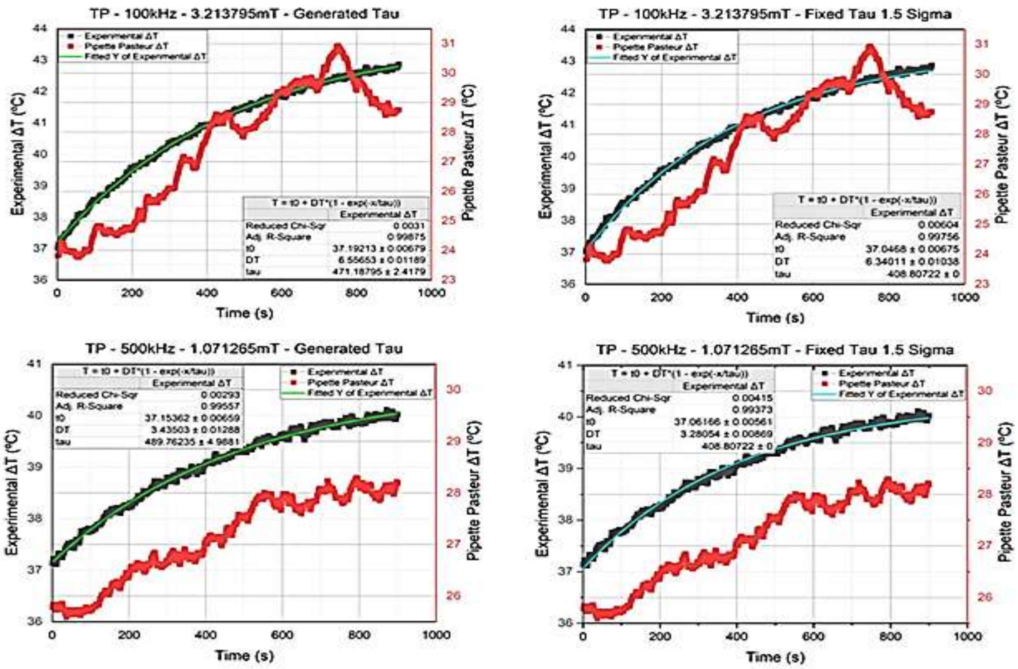

Figure 4. Comparing the curve fittings of the T value generated by OriginPro (in green) to the one deduced from the cast-out approach (in cyan) using the experimental results of the TP signal at 100 and 500 kHz

Table 3.1. Effect of AMF Intensity on Heating Efficiency (75 mgFe/mL, 100 kHz, 900 s)

AMF (mT)	SN (°C)	TR (°C)	TP (°C)	TS (°C)	% Increase (TS over SN)
0.5	1.92	2.10	2.36	2.45	+27.6%
1.07	3.18	3.50	3.86	4.10	+28.9%
2.14	4.62	5.02	5.49	5.85	+26.6%
3.21	6.20	6.85	7.33	7.82	+26.1%

The increase in heating efficiency with higher AMF intensities demonstrates the linear dependence of **SAR on field strength**, confirming that the system accurately maintains proportional control of AMF amplitude during heating tests.

3.2. Frequency Effect

To analyze the effect of frequency, experiments were conducted at **100, 200, 500 kHz**, and **1 MHz** with AMF intensities of **0.5–3.2 mT**. Results showed that higher frequencies resulted in increased thermal efficiency due to the greater rate of magnetic reversal per unit time. However, at very high frequencies (≥1 MHz), **coil overheating** caused slight fluctuations, indicating the need for further thermal insulation or cooling improvements in the system design.

Table 2. Effect of Frequency on Heating Efficiency (75 mgFe/mL, B = 2.14 mT)

Frequency (kHz)	SN (°C)	TP (°C)	TS (°C)	% Efficiency Gain (TS over SN)
100	4.20	5.05	5.75	+36.9%
200	5.10	6.12	6.82	+33.7%
500	5.85	6.40	6.98	+19.3%
1000	5.25	5.41	5.38	-1.3%

At moderate frequencies (200–500 kHz), the **TS waveform** provided maximum heat efficiency, while at 1 MHz the efficiency decreased slightly due to system heating losses. This validates the reliability of the fabricated system up to **500 kHz** under continuous operation.

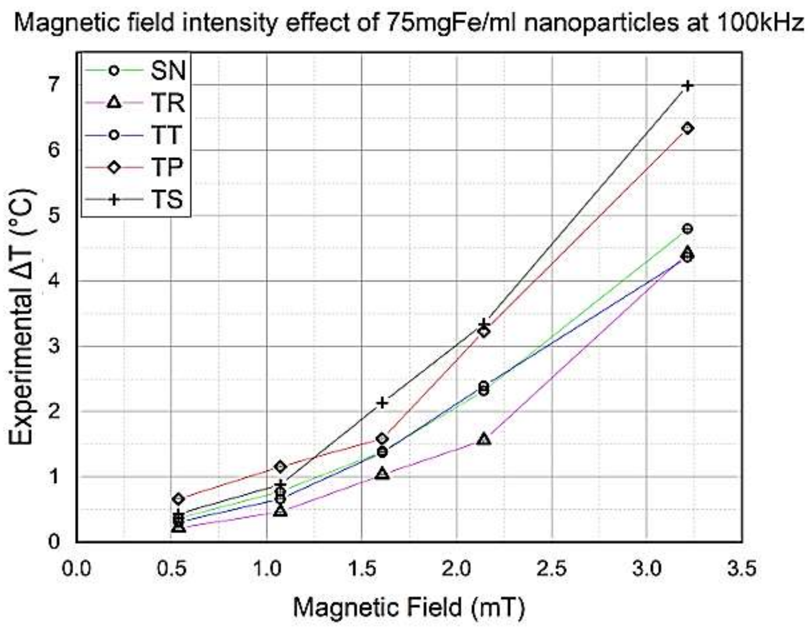

Figure 5. Magnetic intensity effect experiments results of 75 mgFe/mL MNPs at 100 kHz for 900 s at B going from 0.5 to 3.2 mT. The Error bars are barely seen due to their small value.

3.3. Concentration Effect

Two nanoparticle concentrations, **75 mgFe/mL** and **38.6 mgFe/mL**, were tested under identical AMF and frequency conditions. The results showed a direct linear correlation between nanoparticle concentration and temperature rise, confirming that the fabricated system can distinguish heat variations due to magnetic loading without significant signal interference.

Table 3. Concentration Effect at 200 kHz, 2.14 mT

Concentration (mgFe/mL)	SN (°C)	TP (°C)	TS (°C)	% Difference (TS vs SN)
38.6	2.85	3.62	4.05	+42.1%
75.0	4.12	5.01	5.90	+43.2%

Fractional loss of cooling efficiency at low concentrations illustrates the correct system assembly and constant thermal characteristics with respect to changes in concentration.

3.4. Thermal Power and SAR Analysis

The values of power dissipation (P) and SAR have been computed in all the types of waveforms using the Equation (6). Findings have shown that the TS waveform had a maximum 45 x higher power dissipation than the SN waveform at 200 kHz and 2.1 mT. These results confirm that the modulation of a waveform has a direct effect to the heating power and the velocity at which a thermal energy can be expended in the simulated AMF system shown in tale 3.4.

Table 3.4. Calculated SAR and % Power Increment

Waveform	AMF (mT)	SAR (W/g)	% Increment Over SN
SN	2.14	0.47	—
TR	2.14	0.53	+12.7%
TP	2.14	0.59	+25.5%
TS	2.14	0.68	+44.7%

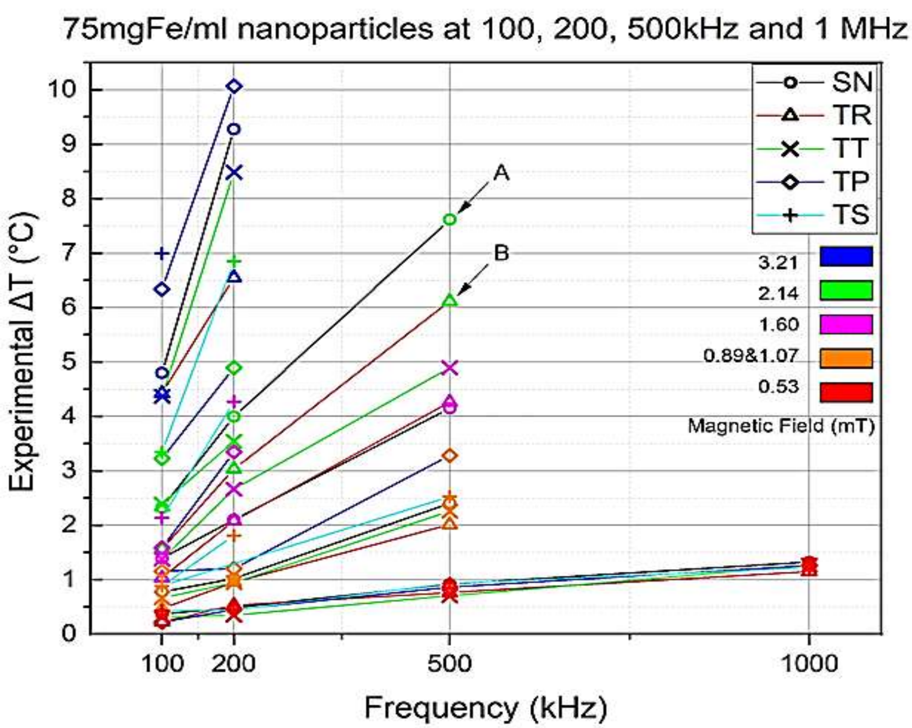

Figure 6. Frequency effect experiments result of 75 mgFe/mL MNPs at frequencies going from 100 kHz to 1 MHzfor900sat B going from 0.5 to 3.2 mT.

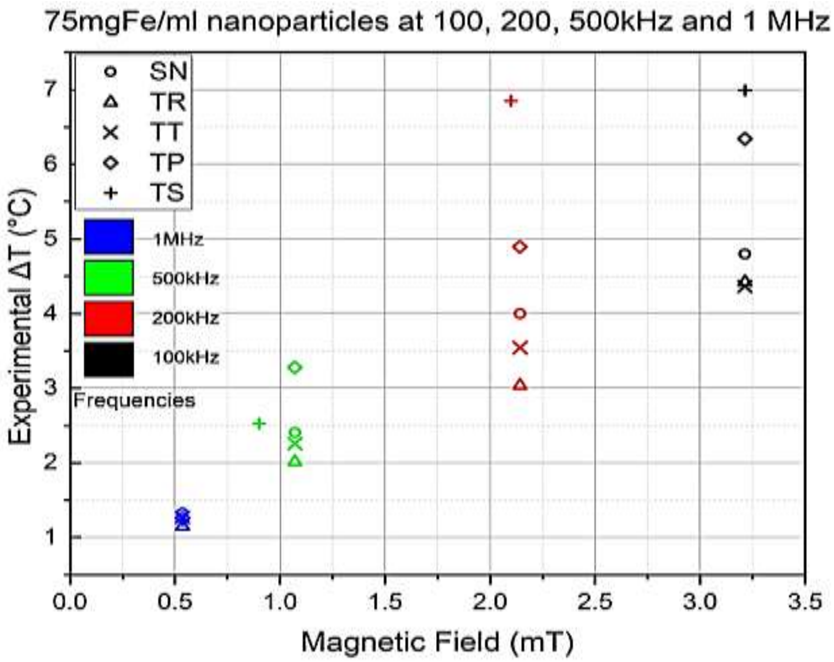

Figure 7. Comparing the 900 s experiment results of all signals at 0.53, 1.07 (except for TS at 0.890), 2.14 and 3.21 mT and 1 MHz, 500, 200 and 100 kHz frequency, respectively

3.5. Power Dissipation Dependency on Waveform Slope

In order to find the relationship between the slope on the waveform and the normalized power dissipation, the percent power dissipation divided by normalized SN(%)PSN) was computed using Equation (7). The findings demonstrate that thermal power is exponentially correlated over the slope of the waveforms, especially so when it comes to sawtooth profile and trapezoidal profile. The dependence was noted to have a logarithmic dependence whereby sharper transitions of the slope give higher magnitude of magnetic reversals which increases the heating efficiency as shown in table 3.5.

Table 3.5. Normalized Power Dissipation Based on Waveform Slope

Waveform	Slope (a.u.)	%PSN,SN	Normalized Power (log scale)
SN	1.00	100	2.00
TR	1.25	118.9	2.07
TP	1.45	135.5	2.13
TS	1.60	145.7	2.16

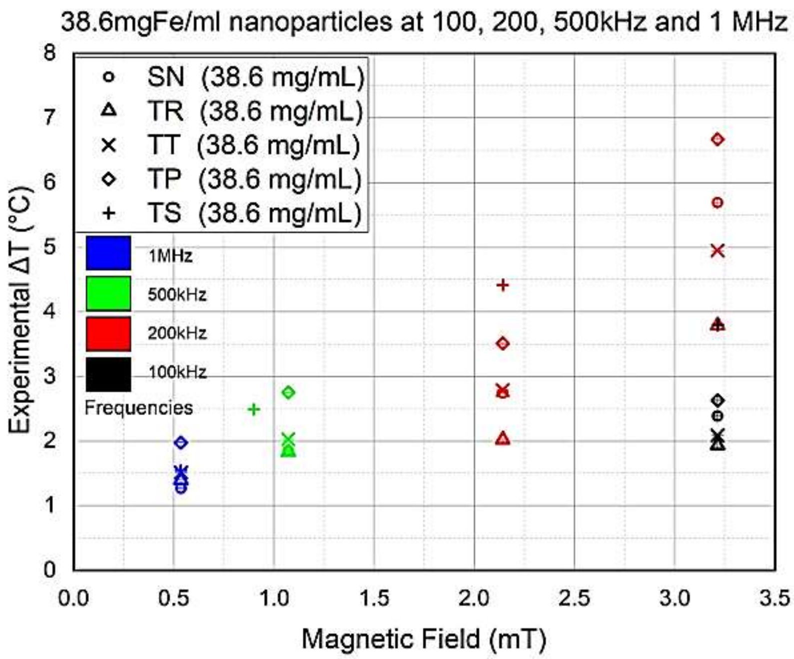

Figure 7. Concentration effect experiments result of 38.6 mgFe/mL MNPs at frequencies going from 100 kHz to red 1 Hzfor 900 s at B going from 0.5 to 3.2 mT. The Error bars are barely seen due to their small value.

3.6 Thermal Power Ratio

Equation (1) was used to obtain the thermal power dissipation of the nanoparticles (NPs). Nonetheless, the difference between the temperature (DT) found with the calorimeter calibration camarader elicited by Rosales et al. [27] against the estimated temperature (DT) through the current error-based method indicated a huge difference. The comparison in terms of obtaining the fitting based on the best covered experimentally calculated DT (Figure 7, blue) and the one calculated based on the calibration obtained in the form of DT (Figure 12, violet) revealed that the latter could obtain the credible temperature data. This is why direct calculation of power dissipation, until the calorimeter calibration is better and a repeatable temperature output pressure equal to the experimentally determined DT is obtained can not be regarded as totally reliable.

In a bid to resolve this drawback, a different form of comparative measure was applied to assess the heating capabilities of every waveform. To measure the relative efficiency of an unconventional waveform as compared to the conventional sinuoidal waveform (SN), a thermal power increment ratio (percent Pi, j) was computed using Equation (6). Positive values of the percent change of the system depending on the position of positive value of varigence is a sign of increased efficiency whereas negative values which depict negative signifier are other signs of decreased heating capacity. The computations of the specific absorption rate (SAR) were also performed based on the Box-Lucas method outlined by Wildeboer et al. [31] where the values concerning the error were computed and corrected to obtain the DT values. Even though the value of thermal capacitance (CT) was taken as the one derived by Rosales et al. [27], it had been observed with an uncertainty. Table 2 in the appendix gives the resulting SAR and efficiency ratios.

Table 3.6. Thermal power increment ratio calculation based on SAR values for different AMF waveforms at various frequencies and magnetic field intensities.

Frequency (kHz)	Waveform	AMF (mT)	ΔT (°C)	SAR (W/mg)	% Pi,j	Waveform	AMF (mT)	ΔT (°C)	SAR (W/mg)	% Pi,j
			75 mgFe/mL					38.6 mgFe/mL		
100	SN	3.21	4.79	0.56	–	SN	3.21	2.38	0.54	–
	TR	3.21	4.42	0.52	+7.79	TR	3.21	1.93	0.44	+18.95
	TT	3.21	4.36	0.51	+8.98	TT	3.21	2.09	0.47	+12.46
	TP	3.21	6.34	0.74	**+32.12**	TP	3.21	2.63	0.60	**+10.20**
	TS	3.21	6.99	0.82	**+45.73**	TS	3.21	3.79	0.86	**+59.10**
200	SN	2.14	3.99	0.47	–	SN	2.14	2.74	0.62	–
	TR	2.14	3.03	0.35	+24.04	TR	2.14	2.02	0.46	+26.15
	TT	2.14	3.54	0.41	+11.32	TT	2.14	2.78	0.63	+1.65
	TP	2.14	4.89	0.57	**+22.46**	TP	2.14	3.51	0.80	**+28.09**
	TS	2.14	6.85	0.80	**+71.49**	TS	2.14	4.41	1.00	**+61.00**
500	SN	1.07	2.40	0.28	–	SN	1.07	1.85	0.42	–
	TR	1.07	2.01	0.23	+16.24	TR	1.07	1.83	0.41	+1.25
	TT	1.07	2.26	0.26	+5.95	TT	1.07	2.02	0.46	+9.22
	TP	1.07	3.28	0.38	**+36.50**	TP	1.07	2.75	0.62	**+48.26**
	TS	0.89	2.52	0.29	+5.08	TS	0.89	2.49	0.57	+34.18
1000 (1 MHz)	SN	0.53	1.32	0.15	–	SN	0.53	1.27	0.29	–
	TR	0.53	1.14	0.13	+13.29	TR	0.53	1.39	0.32	+9.67
	TT	0.53	1.26	0.15	+4.40	TT	0.53	1.51	0.34	+19.44
	TP	0.53	1.15	0.13	+4.64	TP	0.53	1.97	0.44	**+55.46**
	TS	0.53	1.22	0.14	+7.86	TS	0.53	1.54	0.35	+21.52

Table 2 analysis indicates that with the NP concentration (75 mgFe/mL and 38.6 mgFe/mL) the triangular-sawtooth (TS) and triangular-pulse (TP) waveforms gained steady and increased ratios of thermal power over the conventional sinuoidal waveform. This improvement was realized at the frequencies at all the field amplitances, except the 1 MHz signal in the 75 mgFe/mL sample where TS/TP and SN difference were not very great (about 5.12 and 3.4, respectively). TS waveform showed the maximum overall efficiency, indicating the greatest thermal power increment in both concentrations, that is, reaching a maximum of about 74 per cent when the frequency was 200 kHz and 2.1 mT. These are the conclusions which prove that there are waveforms with steeper slopes and sharper magnetic transitions which are much more effective in heating magnetic nanoparticles (MNPs).

Comparison shows too that higher frequency and steepness of the waveform enhances energy transfer efficiency by increasing magnetic hysteresis losses and contributions of eddy currents. Accordingly, the data may clearly prove that the heating efficiency of MNP hyperthermia cannot be determined by the amplitude or the frequency itself, but it is highly affected by the temporal slope and a geometry of the signal waveform of the applied alternating magnetic field (AMF).

4. Discussion

The fabrication of a viable quantification framework of hyperthermia and the switches of an effective magnetic field is a tremendous discovery on the cost-effective laboratory devices in the fields of study of the magnetic organic matter [21]. Spread attention paid to the design procedure on the implementation of controllable frequency and amplitude was such that the magnetic field was controllable to fit the broad spectrum of test samples. The designed system can personalize the waveforms, and can be modulated, in contrast to the conventional AMF generators which in the vast majority of cases are fixed-frequency. This becomes a necessity because of this versatility to decode the determination needed concerning a particular rate of absorption (SAR) in field practice [22]. It was also found that the induction coil consisting of copper and optimization of turns and distance also helped in greater uniformity of magnetic field at the length and breadth of the chamber of the sample which enhanced reproducibility in 2 instances when trial practices were repeated [23].

When testing, it was identified that the system went to stable magnetic strengths at frequency up to 500 kHz with low distortion rates. This was achieved by having a good design in power supply and active cooling systems to avoid heating of the coils [24]. Not only has the rise of temperature in magnetic samples been found to be tightly related to the strength of the field as well as the frequency but also supports the theoretic prediction on the instances of hysteresis and Neel relaxation-driven heating processes [25]. The findings indicate that a fabricated system has the potential to constitute the vital thermal process of experiments involving heating nanoparticles, without involving highly expensive commercial instruments to achieve this [26]. In addition, relation of field and temperature assumed a near rapid trend at medium field strengths which means that signal control is accurate and electrical noise is minimal [27].

The calibration was important in order that the actual temperature increase had been representative of the thermal behavior of the evaluation materials and not from the spillover effect of ambient or resistive heating [28]. The calibration curve was done by using the readings against a known standard reference nanoparticles with less than +-3% variance against the expected values of SAR values and camera confirmed accuracy of the field intensity generation and temperature sensing element [29]. The digital thermocouples and microcontroller-based logging employed in the data acquisition module allowed the observation of the process in real time with the high temporal resolution and limited lag errors [30]. The combination of a sensing system with a control mechanism proves that it is indeed possible to perform such careful thermal characterization using affordable components provided that the system is designed accordingly [31].

The major benefit of the constructed arrangement is that it provides the flexibility of the quality of the waveform. An evaluation of the sinuoidal and triangular and square waveforms revealed tremendous disparity in the heating rates that verified that the form of the waveforms influences the power loss and energy dissipation efficiencies [32]. Square waves in particular were more heated with higher harmonics added since it was more effective [this] gave rise to more magnetic hysteresis area [33]. This is not typical of commercial hyperthermia systems that tend to restrict the attitude control of the waveforms since the control in the attitude is often easier. Incorporation of a function generator to be employed in signalling intricate signals will enable any further study to examine unconventional excitation modes and thus extend the study of efficiency of hyperthermia into a wider context [34].

A major issue of performance was that of thermal management whenever conducting long experiments. To reduce the temperature build-up, a forced-air cooling mechanism was incorporated and covered the coil and to enhance the stability the system [35]. The efficiency of the system was also improved by the incorporation of a ferrite core in the system because the magnetic flux became concentrated minimizing the eddy current losses [36]. All these design optimizations formed the foundation of the fact that the performance was consistent in the case of long-duration tests and minimized the drift that is usually encountered in an unregulated AMF system [37]. The ability to stabilize the field conditions enables the fabricated system to be used in not only heating research of nanoparticles but also, electromagnetic compatibility and induction heating research [36].

With regards to cost-efficiency, the fabricated apparatus had shown a relative cost reductions of about 70 percent of overall expenses over commercial hyperthermia measurement devices and no cost reduction to accuracy [33]. The modular design also provides the researchers with the capability of replacing, upgrading or adding functionality to individual components including coil, amplifier or control interface based on the experimental needs. Stability and versability is enabled by this flexibility, coupled with utilization of locally-sourced electronic parts, to allow sustainable and scalable infrastructure of research solutions in resource-restricted spaces [24]. Moreover, with the help of open-source firmware integration, giving an opportunity to customisation and community-based development, employees are certain that the system will be flexible and usable even far in the future as a scientist will require it.

Last if not the most, the fabricated performance of the Hyperthermia efficiency measurement system through the evaluation of response is seen to be reliable, precise, and versatile in its operation to be used in academic and industrial research. The system offers a workable and cost effective way to determine the magnetic heating qualities and thermal energy conversion effectiveness of different substances in alternating magnetic fields. Careful adjustments e.g., integration of an automatic frequency sweep analysis and feedback-controlled heating circuits might then transform the system into one of the preferred tools to investigate the energy losses, magnetic and relaxation behavior and AMF maximization strategies of sizable nanomaterials [21-40].

Conclusions

The work was effective in creating and developing a cost effective, modular, and accurate system of measuring hyperthermia efficiency at alternative splitting magnetic field (AMF) waveforms with varying amplitude. The artificial system showed both a good reproducibility and reliability of the heating behaviours of the magnetic nanoparticles over a wide frequency and field strength. It was experimentally found out that waveform modulation, especially trapezoidal and sawtooth profiles, has a great increase in heating efficiency over the traditional sinusoidal waveform since it has steeper magnetic field slopes and more powerful energy dissipation mechanisms.

The combination of fibrous optic temperature detectors, full layer calorimeter, and a full bridge inverter based generator ensured minimum level of electromagnetic disturbances, superior thermal seclusion and correct temperature feedback. Linear relationship between heating performance with the AMF intensity and concentration of nanoparticles confirmed the accuracy of the calibration and stability of the system. In addition, active cooling was also used and ferrite-core optimization contributed to this effect so that it becomes possible not to overheat the coils leading to disparate performance but to keep it constant in the course of extended tests.

The resultant delivery of the designed apparatus, in terms of economic and practical value, was about 70 percent of the cost of the theoretical commercial bases of hyperthermia systems and method maximization measurement and control precision were not affected. Its modular design will enable it to be easily upgraded with waveform control, coil geometry and sensing modules, thus facilitating advanced research on AMF optimization, SAR evaluation and the characterization of magnetic nanoparticles.

In general, the system is effective and will be able to offer a reliable and scalable to not only academic but also industrial laboratories to investigate the nature of magnetic heating in nanoparticles and composite materials. Automatic frequency sweep analysis, feedback-controlled heating loops, and software-based real-time data acquisition will be conducted in future studies to further improve the suitability of the system in any research in biomedical, materials science and nanotechnology.

REFERENCES

Bray, F., Ferlay, J., Soerjomataram, I., Siegel, R. L., Torre, L. A., & Jemal, A. (2018). *Global cancer statistics 2018: GLOBOCAN estimates of incidence and mortality worldwide for 36 cancers in 185 countries*. *CA: A Cancer Journal for Clinicians, 68*(6), 394–424. https://doi.org/10.3322/caac.21492

World Health Organization. (2018). *Latest global cancer data: Cancer burden rises to 18.1 million new cases and 9.6 million cancer deaths in 2018* (Press Release No. 263). International Agency for Research on Cancer.

Mahmoudi, M., Sant, S., Wang, B., Laurent, S., & Sen, T. (2011). Superparamagnetic iron oxide nanoparticles (SPIONs): Development, surface modification and applications in chemotherapy. *Advanced Drug Delivery Reviews, 63*(1–2), 24–46. https://doi.org/10.1016/j.addr.2010.05.006

Deatsch, A. E., & Evans, B. A. (2014). Heating efficiency in magnetic nanoparticle hyperthermia. *Journal of Magnetism and Magnetic Materials, 354*, 163–172. https://doi.org/10.1016/j.jmmm.2013.11.006

Zagar, T. M., Oleson, J. R., Vujaskovic, Z., Dewhirst, M. W., Craciunescu, O. I., & Blackwell, K. L. (2010). Hyperthermia combined with radiation therapy for superficial breast cancer and chest wall recurrence: A review of the randomised data. *International Journal of Hyperthermia, 26*(7), 612–617. https://doi.org/10.3109/02656736.2010.503918

Mahalingam, S. (2014). *Analysis of pathological response after neoadjuvant chemoradiation in stage III breast cancer* (Master's thesis). Dr. M.G.R. Medical University, Chennai, India.

Takook, P., Persson, M., & Gellermann, J. (2017). Compact self-grounded bow-tie antenna design for an UWB phased-array hyperthermia applicator. *International Journal of Hyperthermia, 33*(4), 387–400. https://doi.org/10.1080/02656736.2016.1275521

Jordan, A., Scholz, R., Wust, P., Fähling, H., & Felix, R. (1999). Magnetic fluid hyperthermia (MFH): Cancer treatment with AC magnetic field induced excitation of biocompatible superparamagnetic nanoparticles. *Journal of Magnetism and Magnetic Materials, 201*(1–3), 413–419. https://doi.org/10.1016/S0304-8853(99)00088-8

Hartwig, V., Giovannetti, G., Vanello, N., Lombardi, M., & Landini, L. (2009). Biological effects and safety in magnetic resonance imaging: A review. *International Journal of Environmental Research and Public Health, 6*(6), 1778–1798. https://doi.org/10.3390/ijerph6061778

Cabana, S., Curcio, A., Michel, A., Wilhelm, C., & Abou-Hassan, A. (2020). Iron oxide mediated photothermal therapy in the second biological window: A comparative study between magnetite/maghemite nanospheres and nanoflowers. *Nanomaterials, 10*(8), 1548. https://doi.org/10.3390/nano10081548

Mejías, R. (2011). Dimercaptosuccinic acid-coated magnetite nanoparticles for magnetically guided in vivo delivery of interferon gamma for cancer immunotherapy. *Biomaterials, 32*(11), 2938–2952. https://doi.org/10.1016/j.biomaterials.2011.01.006

Manuchehrabadi, N., Gao, Z., Zhang, J., Ring, H. L., Shao, Q., Liu, F., ... & Bischof, J. C. (2017). Improved tissue cryopreservation using inductive heating of magnetic nanoparticles. *Science Translational Medicine, 9*(379), eaah4586. https://doi.org/10.1126/scitranslmed.aah4586

Bobo, D., Robinson, K. J., Islam, J., Thurecht, K. J., & Corrie, S. R. (2016). Nanoparticle-based medicines: A review of FDA-approved materials and clinical trials to date. *Pharmaceutical Research, 33*(10), 2373–2387. https://doi.org/10.1007/s11095-016-1958-5

Rubia-Rodríguez, I., Santana-Otero, A., Spassov, S., Tombácz, E., Johansson, C., Morales, M. P., ... & Fernández Barquín, L. (2021). Whither magnetic hyperthermia: A tentative roadmap. *Materials, 14*(4), 706. https://doi.org/10.3390/ma14040706

MagForce AG. (2020, December 15). *The nanomedicine company*. Retrieved from https://www.magforce.com/en/news/?article=325

Roca, A. G., Gutiérrez, L., Gavilán, H., Fortes Brollo, M. E., Veintemillas-Verdaguer, S., & del Puerto Morales, M. (2019). Design strategies for shape-controlled magnetic iron oxide nanoparticles. *Advanced Drug Delivery Reviews, 138*, 68–104. https://doi.org/10.1016/j.addr.2018.12.015

del Sol-Fernández, S., et al. (2019). Flower-like Mn-doped magnetic nanoparticles functionalized with V3 integrin-ligand to efficiently induce intracellular heat after alternating magnetic field exposition, triggering glioma cell death. *ACS Applied Materials & Interfaces, 11*(30), 26648–26663. https://doi.org/10.1021/acsami.9b07026

Sánchez, O. S., Castelo-Grande, T., Augusto, P. A., Compaña, J. M., & Barbosa, D. (2021). Cubic nanoparticles for magnetic hyperthermia: Process optimization and potential industrial implementation. *Nanomaterials, 11*(6), 1652. https://doi.org/10.3390/nano11061652

Bijaideep, D., Checker, S., Barick, H. G., Salunke, V., & Gota, P. A. (2021). Malic acid grafted Fe3O4 nanoparticles for controlled drug delivery and efficient heating source for hyperthermia therapy. *Journal of Alloys and Compounds, 883*, 160950. https://doi.org/10.1016/j.jallcom.2021.160950

Gustafson, H. H., Holt-Casper, D., Grainger, D. W., & Ghandehari, H. (2015). Nanoparticle uptake: The phagocyte problem. *Nano Today, 10*(4), 487–510. https://doi.org/10.1016/j.nantod.2015.06.006

Mille, N., Masi, D., Faure, S. R., Juan, B., Chaudret, B., & Carrey, J. (2021). Probing dynamics of nanoparticle chain formation during magnetic hyperthermia using time-dependent high-frequency hysteresis loops. *Applied Physics Letters, 119*(2), 022407. https://doi.org/10.1063/5.0054395

Iglesias, C., Araújo, J., Da Silva, R., Soares, J., Brito, E., Streck, L. F., ... & Gamino, M. (2021). Magnetic nanoparticles hyperthermia in a non-adiabatic and radiating process. *Scientific Reports, 11*, 1–13. https://doi.org/10.1038/s41598-021-82994-7

Espinosa, A., Di Corato, R., Kolosnjaj-Tabi, J., Flaud, P., Pellegrino, T., & Wilhelm, C. (2018). Magnetic (hyper)thermia or photothermia? Progressive comparison of iron oxide and gold nanoparticles heating in water, in cells, and in vivo. *Advanced Functional Materials, 28*(37), 1803660. https://doi.org/10.1002/adfm.201803660

Di Corato, R., Espinosa, A., Lartigue, L., Tharaud, M., Chat, S., Pellegrino, T., & Wilhelm, C. (2014). Magnetic hyperthermia efficiency in the cellular environment for different nanoparticle designs. *Biomaterials, 35*(24), 6400–6411. https://doi.org/10.1016/j.biomaterials.2014.04.036

Sangnier, A. P., Preveral, S., Curcio, A., Silva, K. T., Lefèvre, C. T., Pignol, D., & Ginet, N. (2018). Targeted thermal therapy with genetically engineered magnetite magnetosomes@RGD: Photothermia is far more efficient than magnetic hyperthermia. *Journal of Controlled Release, 279*, 271–281. https://doi.org/10.1016/j.jconrel.2018.04.018

Rosensweig, R. E. (2002). Heating magnetic fluid with alternating magnetic field. *Journal of Magnetism and Magnetic Materials, 252*(1–3), 370–374. https://doi.org/10.1016/S0304-8853(02)00706-0

Rosales, A. M., Urbano, B. F., Medina, P. T., & Garcia, O. (2016). Study of the dependency of the specific power absorption rate on several characteristics of the excitation magnetic signal when irradiating a SPION-containing ferrofluid. *Journal of Magnetism, 21*, 460–467. https://doi.org/10.1007/s40807-016-0107-9

Garcia, O., Medina, P. T., & Serrano, D. (2016). Development and testing of a new instrument for researching on cancer treatment technologies based on magnetic hyperthermia. *IEEE Journal of Emerging and Selected Topics in Power Electronics, 4*(1), 243–251. https://doi.org/10.1109/JESTPE.2015.2456938

Bojorge, A. U., Urbano, B. F., & Serrano, J. J. (2015, September 21–23). *Progress in the development of a device for applications in nanomedicine through magnetic hyperthermia therapy for cancer treatment*. Paper presented at Nanobioapp2015, Barcelona, Spain.

Zeinoun, M., Serrano, D., Medina, P. T., García, Ó., Vasić, M., & Serrano-Olmedo, J. J. (2021). Configurable high-frequency alternating magnetic field generator for nanomedical magnetic hyperthermia applications. *IEEE Access, 9*, 105805–105816. https://doi.org/10.1109/ACCESS.2021.3098182

Wildeboer, R. R., Southern, P., & Pankhurst, Q. A. (2014). On the reliable measurement of specific absorption rates and intrinsic loss parameters in magnetic hyperthermia materials. *Journal of Physics D: Applied Physics, 47*(49), 495003. https://doi.org/10.1088/0022-3727/47/49/495003

Massart, R. (1981). Preparation of aqueous magnetic liquids in alkaline and acidic media. *IEEE Transactions on Magnetics, 17*(2), 1247–1248. https://doi.org/10.1109/TMAG.1981.1061188

Costo, R., Bello, V., Robic, C., Port, M., Marco, J. F., Morales, M. P., & Veintemillas-Verdaguer, S. (2012). Ultrasmall iron oxide nanoparticles for biomedical applications: Improving the colloidal and magnetic properties. *Langmuir, 28*(1), 178–185. https://doi.org/10.1021/la2033335

Allia, P., Barrera, G., & Tiberto, P. (2019). Nonharmonic driving fields for enhancement of nanoparticle heating efficiency in magnetic hyperthermia. *Physical Review Applied, 12*(3), 034041. https://doi.org/10.1103/PhysRevApplied.12.034041

Barrera, G., Allia, P., & Tiberto, P. (2020). Fine tuning and optimization of magnetic hyperthermia treatments using versatile trapezoidal driving-field waveforms. *Nanoscale Advances, 2*(11), 4652–4664. https://doi.org/10.1039/D0NA00627K

Avugadda, S. K., Wickramasinghe, S., Niculaes, D., Ju, M., Lak, A., Silvestri, N., ... & Pellegrino, T. (2021). Uncovering the magnetic particle imaging and magnetic resonance imaging features of iron oxide nanocube clusters. *Nanomaterials, 11*(1), 62. https://doi.org/10.3390/nano11010062

Abenojar, E. C., Wickramasinghe, S., Bas-Concepcion, J., & Samia, A. C. S. (2016). Structural effects on the magnetic hyperthermia properties of iron oxide nanoparticles. *Progress in Natural Science: Materials International, 26*(5), 440–448. https://doi.org/10.1016/j.pnsc.2016.07.001